Journal of Power Sources 209 (2012) 105–119

Contents lists available at SciVerse ScienceDirect

Journal of Power Sources

journal homepage: www.elsevier.com/locate/jpowsour

Direct solar photovoltaic charging of a high voltage nickel metal hydride traction battery

Nelson A. Kelly*

General Motors R&D Center, 480-106-224, Chemical Sciences and Materials Systems Laboratory, 30500 Mound Road, Warren, MI 48090-9055, USA

ARTICLE INFO

Article history:
Received 26 January 2012
Received in revised form 21 February 2012
Accepted 23 February 2012
Available online 6 March 2012

Keywords:
Photovoltaic (PV)
High voltage battery
Solar energy
Electric vehicles
Optimized system

ABSTRACT

The electrification of vehicle power trains using batteries and fuel cells is an important technological step forward in the effort to improve the efficiency and reduce the tailpipe emissions of vehicles. The production of electricity and hydrogen in a renewable fashion, such as using solar energy, can provide a clean and sustainable energy source for electric-powered vehicles. In the present work we develop a charging system to prove the concept of direct, efficient, solar-powered charging for battery-electric vehicles using solar photovoltaic-powered charging of the high-voltage nickel-metal hydride (NiMH) battery that is used in the GM 2-mode hybrid system. We utilize a protocol for high-voltage battery charging that was developed in an earlier study that included a DC–DC converter to boost the low-voltage produced by the PV array to the high voltage needed to charge the battery. However, no power conversion was used in the present study. Rather, we use a high-voltage solar array capable of outputting a wide range of voltages, from approximately 250 to 400 V in 50 V increments, at the photovoltaic system maximum power point. By varying the solar system output voltage we measured the solar energy to battery charging efficiency under a variety of conditions to determine the optimal photovoltaic system configuration. The system and methods developed in this work can be used to efficiently charge a range of battery electric vehicles by adapting the PV system output to the battery charging voltage.

1. Introduction

In order to increase vehicle efficiency, reduce dependence on petroleum, and reduce emissions of air pollutants and greenhouse gases, there is an increasing trend toward vehicle electrification. This move toward electric power trains is part of the "new DNA" for future vehicles [1–4]. At General Motors (GM) we are pursuing this goal by developing a test fleet of fuel cell electric vehicles (FCEV) powered by hydrogen [1,2] as well as marketing a range of electrified vehicles, from hybrid electric vehicles (HEV) to plug in and extended range electric vehicles (PHEV and EREV) in which internal combustion engines and electric motors are both utilized [5,6] to achieve the aforementioned goals.

In order to have a sustainable transportation system it is important that vehicles are powered by renewable energy. In support of this long-term goal we have studied the production of hydrogen for FCEV [7–11] and electricity for battery charging [11–13] using solar energy. Solar energy has the potential to supply an ever increasing fraction of the total energy needed in the future and in particular the DC electricity produced by solar photovoltaic (PV) cells, modules, and arrays is ideally suited to split water to produce hydrogen and to charge batteries [14–16]. Solar powered hydrogen and battery charging systems can be scaled from small widely distributed systems, including individual home owners and parking structures [11], to large-scale installations that collect the solar energy from hundreds of square miles of land and store it as chemical energy in charged batteries or as hydrogen produced via water electrolysis [15–19]. Solar energy can provide a clean, renewable source of energy to charge PHEV, EREV, and battery electric vehicles (BEV) to maximize the environmental benefits of eliminating greenhouse gases and other emissions associated with fossil-fueled electric generation. However, a major challenge to using solar energy technology is the need to design an inexpensive, safe solar battery charger with optimum efficiency.

In our first study on charging a high-voltage traction battery using a PV system we decided to use our low voltage arrays with a DC–DC converter to increase the 50-V output to 350 V necessary to charge the nickel metal hydride (NiMH) used in the GM 2-mode hybrid [13]. That study served as a proof of concept for charging a high-voltage battery with PV electricity. To our knowledge, this was the first time a high-voltage HEV battery was charged using solar energy with charge control provided by the internal battery computer. Because battery packs for electric powered and electric assisted vehicles have electronic controls to monitor and control the charging, the PV system only needs to be designed to have a maximum-power point voltage near the charge cut-off voltage

* Tel.: +1 586 986 1623; fax: +1 586 986 1910.
E-mail address: nelson.a.kelly@gm.com

0378-7753/$ – see front matter © 2012 Elsevier B.V. All rights reserved.
doi:10.1016/j.jpowsour.2012.02.106

Nomenclature

A	amperes
BEV	battery electric vehicle
BPCM	battery pack control module
CAN	controller area network, communication protocol between system components and computers
CAPL	Communication Application Programming Language, used to control the battery charging and discharging (Table 2)
DAQ	data acquisition system
EREV	extended range electric vehicle
FCEV	fuel cell electric vehicle
HEV	hybrid electric vehicle
HVIL	high voltage interlock used to disable battery
I	current, amperes
I_{mpp}	PV maximum power point current, amperes
I_{sc}	PV short circuit current, amperes
MPP	PV maximum power point; at this point the system has P_{max}, V_{mpp}, I_{mpp} and maximum solar to electric efficiency
P_{max}	PV maximum power, W ($=V_{mpp} \times I_{mpp}$)
PHEV	plug-in hybrid electric vehicle
PV	photovoltaic cells, modules, or arrays
SOC	state of charge, %
Solar energy	product of solar insolation and the array area, kWh
Solar insolation	solar irradiance integrated over time, kWh m^{-2}
Solar irradiance	solar flux, power per unit area, kW m^{-2}
SPAPM	Sandia photovoltaic array performance model
STC	standard test conditions (for PV cells, modules, or arrays, this is an irradiance of 1000 W m^{-2}, a solar spectrum referred to as AM1.5, and a temperature of 25 °C)
T_{array}	PV module temperature, °C
V	volts
V_{batt}	battery terminal voltage, approximately equals V_{solar} when the battery is being charged by the PV system, V
$V_{90}(L)$	lower voltage ($<V_{mpp}$) where the PV system puts out 90% of the maximum power, P_{max}, V
$V_{90}(H)$	higher voltage ($>V_{mpp}$) where the PV system puts out 90% of the maximum power, P_{max}, V
V_{mpp}	PV maximum power point voltage, V
V_{oc}	PV open circuit voltage, V
V_{solar}	PV array voltage when charging the battery, V

programmed into the battery pack control module, as described in our earlier work [13]. The system we tested achieved a solar to battery charging efficiency averaging slightly above 13% in six battery charging tests.

Most solar systems employ DC to AC power conversion using an inverter, and then that AC must be converted back to DC if the solar power is used to charge a battery. In the present paper we will describe a series of experiments conducted with a PV system designed so that it could directly charge the NiMH battery with DC current without any power conversion. The impetus for direct DC charging of the vehicle battery using PV-generated electricity is threefold: (1) it takes advantage of the fact that PV system outputs DC current, and thus eliminates the approximately 10% loss for conversion of DC to AC (inverter) and AC back to DC (battery charger), (2) it eliminates the cost of AC–DC power converters, and (3) it could eliminate the weight of the on-board charger in a vehicle such as the Chevrolet Volt, which in turn will reduce vehicle weight and result in a greater vehicle driving range. Thus, a direct DC charging system can improve the system efficiency and lower the cost of a PV battery charging system, as well as improve the vehicle performance.

2. Experimental

The system was designed as a number of units that take solar energy and use it to charge a hybrid electric vehicle (HEV) battery. Some of the parts were used previously, while other parts had to be designed and built in order to charge a high-voltage battery. The following will describe the system components and their interworkings.

2.1. High-voltage solar array

We modified one of the four solar arrays used in our previous work so that it could output the high voltage needed for charging traction batteries, such as the NiMH PEVE battery. A picture of the four solar arrays used in our previous work [7,10,12,13], with the high voltage array labeled, is shown in Fig. 1a. The combiner box on the back of the high-voltage array is shown in Fig. 1b. It was wired so that so that from five to eight 50 V Sanyo HIP190-BA3 photovoltaic (PV) modules (Sanyo Energy Corp., Frisco, TX) in series could be selected and used to charge the high-voltage battery (50 V refers to the approximate maximum power point (MPP) voltage under ambient conditions, discussed later). The wiring scheme is shown in Fig. 2 for ease of explanation. The special high-voltage array had five PV modules wired in series as the minimum basis set, with the option for selecting a sixth, a seventh, or an eighth module to the base set. This was achieved with high voltage relays that brought the additional modules into the circuit depending on the position of the switch on the combiner box. For example, if the selector switch was set to position five, relay 1 in Fig. 2 would be pointing down (connected to the white circle), and five 50 V modules in series would provide an output voltage of approximately 250 V at the PV MPP. If the selector switch was set to position six, relay 1 would be up (connected to the black circle) and relay 2 would be down, so that six modules would be in series to provide an output voltage of 300 V at the MPP. The highest output voltage at the MPP, for eight modules in series, was 400 V. The actual wiring was somewhat more complex than shown in the simplified schematic because opening and closing relays at high DC voltages is prone to arcing. This special high-voltage array allowed us to measure the solar to battery charging efficiency over a wide range of output voltages as shown in Table 1.

Table 1 shows the important parameters for each possible combination of modules in series along with the nominal efficiency and temperature coefficients for the Sanyo HIP-190BA3 PV modules under standard test conditions (STC). For example, at STC one module has an output voltage of 54.8 V. However, typically the PV system temperature was 10–20 °C above the STC temperature of 25 °C, so the MPP voltage for each module was 49.7–53.1 V; for convenience in our discussion we are referring to the modules as 50 V modules.

The high voltage solar array was equipped with a model Li-200SL Li-COR sensor (Li-COR Biosciences, Lincoln, NE) to measure the solar irradiance (Wm^{-2}). The sensor was mounted in the plane of the array. A thermocouple was attached to the back of one module to measure the module temperature. Details on the solar arrays and irradiance measurements are contained elsewhere [21].

2.2. NiMH battery pack

We used the same nickel metal hydride (NiMH) battery pack in the present study as was used in our earlier study [13]. This battery

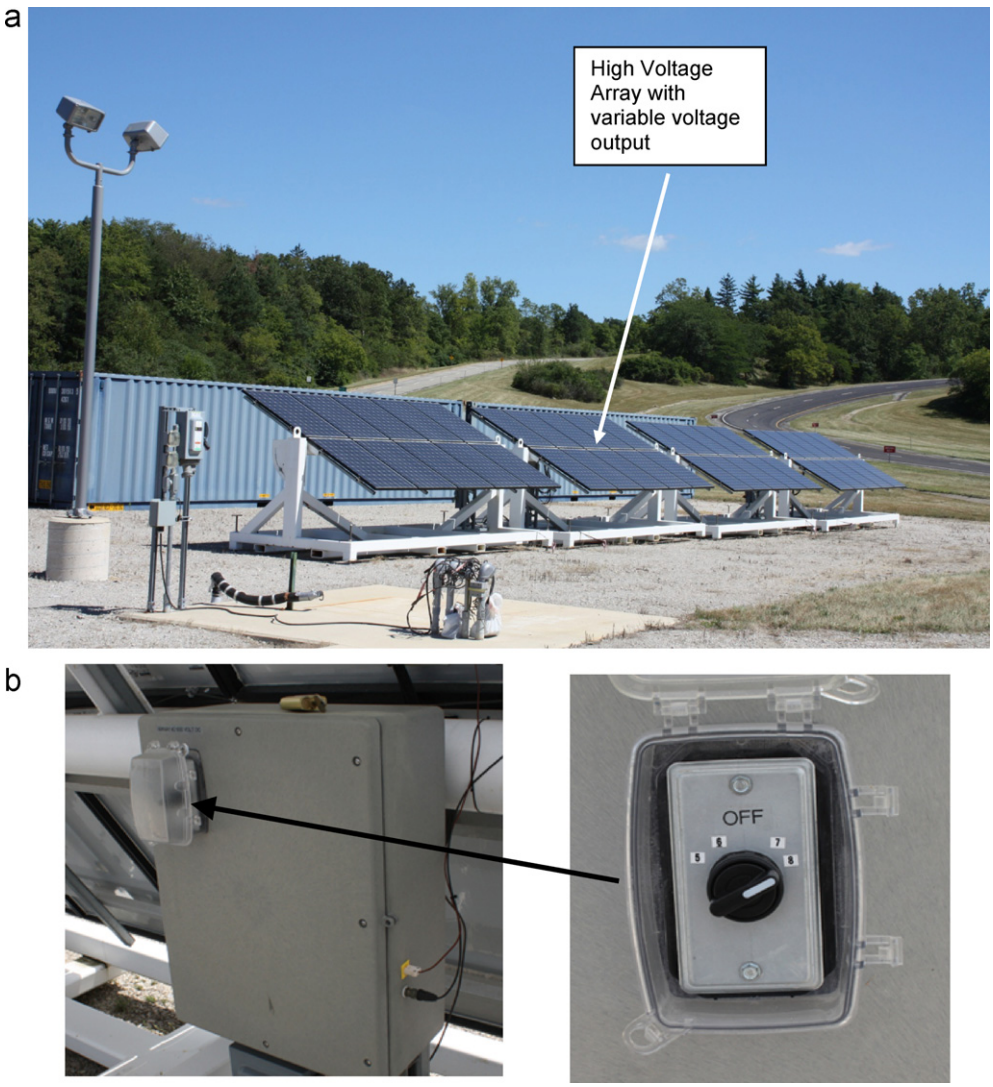

Fig. 1. Solar PV battery charging system at the GM Milford Proving Ground: (a) PV arrays with high-voltage array#2 identified, and (b) selector on the back of the array allowing the choice of five, six, seven, or eight modules in series.

is used in the GM-2-mode hybrid system and referred to as the PEVE battery. It was made by Panasonic EV Energy Co. (now Primearth EV Energy Co, Ltd., Kosai, Shizouka, Japan) [22]. Details on the battery, including the electrochemistry, are given in our earlier report. A picture of the NiMH battery sitting on a table along with other equipment used in the testing is shown in Fig. 3a. Fig. 3b shows some of the internal components of the battery pack. It has 40 prismatic modules connected in series. Each prismatic module consists of six NiMH battery cells wired in series. Battery parameters were measured and reported by the internal battery pack control module (BPCM) for sets of two modules in series called blocks. For example, the voltage of each block was measured, and the maximum and minimum were used to determine when to stop discharging or charging the battery, respectively. The BPCM is shown at the right of Fig. 3b. The BPCM broadcasts important battery parameters on the CAN bus, and the bus is monitored via an 18-pin connector as discussed later. The BPCM also controls the fan cooling the battery pack, based on temperature measurements on some of the

Table 1
Solar PV system parameter nominal values for the high-voltage, variable output array with five to eight modules in series at standard test conditions (STC).[a]

Parameter	$N=5$	$N=6$	$N=7$	$N=8$
Maximum power, P_{max}, W	950	1140	1330	1520
Maximum power point voltage, V_{mpp}, V	274.0	328.8	383.6	438.4
Maximum power point current, I_{mpp}, amperes	3.47	3.47	3.47	3.47
Open circuit voltage, V_{oc}, V	337.5	405.0	472.5	540
Short circuit current, I_{sc}, amperes	3.75	3.75	3.75	3.75
Module efficiency, %	16.1	16.1	16.1	16.1
Temperature coefficient (P_{max}), $\%\,^{\circ}C^{-1}$	−0.30	−0.30	−0.30	−0.30
Temperature coefficient (V_{oc}), $V\,^{\circ}C^{-1}$	−0.169	−0.169	−0.169	−0.169
Temperature coefficient (I_{sc}), $mA\,^{\circ}C^{-1}$	0.86	0.86	0.86	0.86
Total module area, m^2	5.895	7.074	8.253	9.432

[a] Nominal values at standard test conditions (irradiance = 1000 W m^{-2} and module temperature = 25 °C) reported by the manufacturer[20].

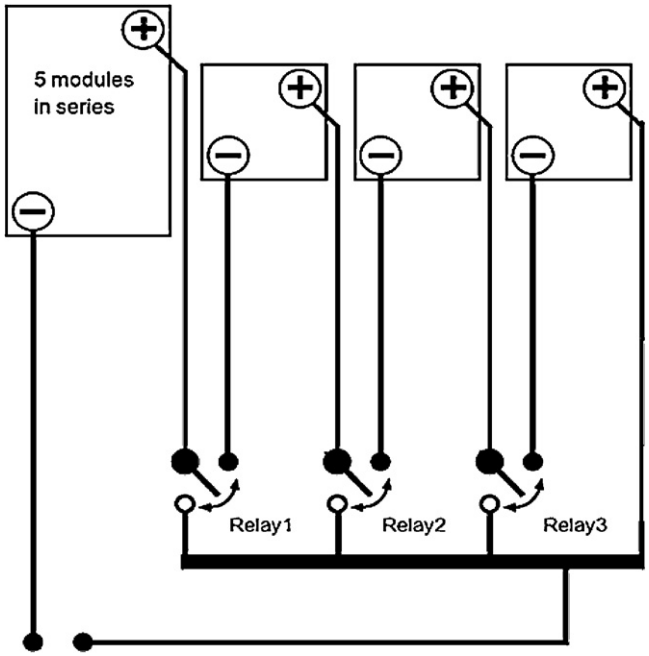

Fig. 2. A schematic of the variable, high-voltage PV battery charging system showing the base system of five Sanyo PV modules in series together with relays to select six, seven, or eight modules in series. This is for illustrative purposes only.

modules, as well as controlling three sets of internal battery high-voltage relays that must be engaged to allow high voltage to be present on the battery output terminals.

2.3. Battery pack activation hardware and software

A picture of the battery pack, hardware associated with controlling the internal battery connectors, a load bank for battery discharging, and a computer for controlling the battery discharging and charging is shown in Fig. 3. To charge or discharge the NiMH battery, three internal high voltage relays or contactors need to be activated so that the output terminals are "live". The first step in this process is installing the manual high voltage safety interlock connectors (HVIL): one is present on the battery terminal cover, and a second safety interlock is inserted and locked in on the side of the battery case, below the output terminals. The second step involves waking up the pack and closing the internal contactors by satisfying the battery pack control module (BPCM) criteria that were programmed into the BPCM memory for the pack installed in a GM 2-mode hybrid vehicle. This was achieved using signals passed to the BPCM through an 18-pin connector on the battery pack. Several of those pins need to have voltages and signals in order for the BPCM to command the pack to wake up and to close the contactors within the battery pack. The hardware to do this is shown in Fig. 3a and consisted of: (1) a 12 V power supply to simulate the low-voltage battery in the GM-2-mode hybrid vehicle, (2) a pulse generator with the appropriate frequency, pulse width modulation, and duty cycle to simulate the vehicle electronic control module that communicates with the BPCM, and (3) a capacitive load needed at battery-pack contact closure to simulate the battery pack placement with a 2-mode hybrid vehicle. The communication is made through the CAN bus terminals on the connector. The communication is bi-directional; commands are sent to the BPCM and battery data is transmitted from the BPCM. The communication was controlled and parameters from the battery were recorded using a Hewlett Packard (Palo Alto, CA) model NC600 Laptop computer running CANalyzer software (Vector CANtech, Novi, MI) described later. In the present study the capacitive load had to be increased to be able to handle over 500 V that is present at the battery terminals when it was connected to a PV system with eight modules in series and the battery contactors opened. In our previous study, the capacitive load could only tolerate a voltage of 450 V.

Table 2
Important battery pack usage parameters for the NiMH battery pack while under control of the BPCM/CAPL program.

Parameter	Low value (fully discharged)	High value (fully charged)
Pack voltage, V	240	340
Block (2-module in series) voltage, V	12	17
Block temperature, °C	2	38

2.4. Battery pack control program

We used CAN access programming language (CAPL) supplied by Vector CANtech, Inc., running under CANalyzer Pro V7.2 to create a customized program to control the PEVE battery wakeup and contact closure. In battery discharge or charge tests, CANalyzer first was started, followed by loading the CAPL program. The PEVE wakeup command was then given, and once the pack was awake, the contactors were closed so the battery terminals were "live". In addition, CAPL was used to set important BPCM parameters that assured a safe and useful change in the battery state of charge (SOC) upon charge or discharge.

The discharge/charge parameters were set in collaboration with GM engineers with experience in charging and discharging the PEVE battery and are identical to those used previously with the PEVE battery [13]. Table 2 lists the important parameters and the values that were set in the CAPL program. These parameters are based on GM experience with the usage limits of the battery pack and specifications set in consultation with the battery pack manufacturer. When any parameter fell outside the window shown in Table 2, the program opened the contactors and terminated whatever process was occurring (battery discharge or charge). For example, if the battery was being discharged, and the minimum block (2-modules in series) voltage fell below 12 V, the contactors were opened and the discharge was terminated. If all 20 blocks were perfectly balanced, the pack voltage would reach a minimum of 240 V on discharge and 340 V on charge before the CAPL program would open the contactors and terminate the function. Due to the tolerance of NiMH batteries to moderate overcharging [22,23] this block-level control (Table 2) is sufficient to safely charge the pack.

2.5. Battery discharging and charging test protocol

Typically, the battery was initially discharged using a load bank (described below) until the contactors opened. The contactors opened when one module fell below the threshold value in Table 2 (12 V). For a best-case scenario, with perfect balance between the 20 2-module blocks, the pack voltage approached 240 V when the discharging experiment was terminated, i.e., all 20 blocks would attain a low voltage of 12 V. However, termination of a discharging experiment could occur prior to the pack reaching 240 V if one block voltage went below 12 V before the other blocks. Following battery discharge, a battery charging test using the solar charging system was begun within an hour or less. The charging experiment progressed until one of the 2-module block voltages exceeded the upper threshold in Table 2 (17 V), or when the pack voltage exceeds 340 V, at which point the contactors opened and the charging experiment was terminated.

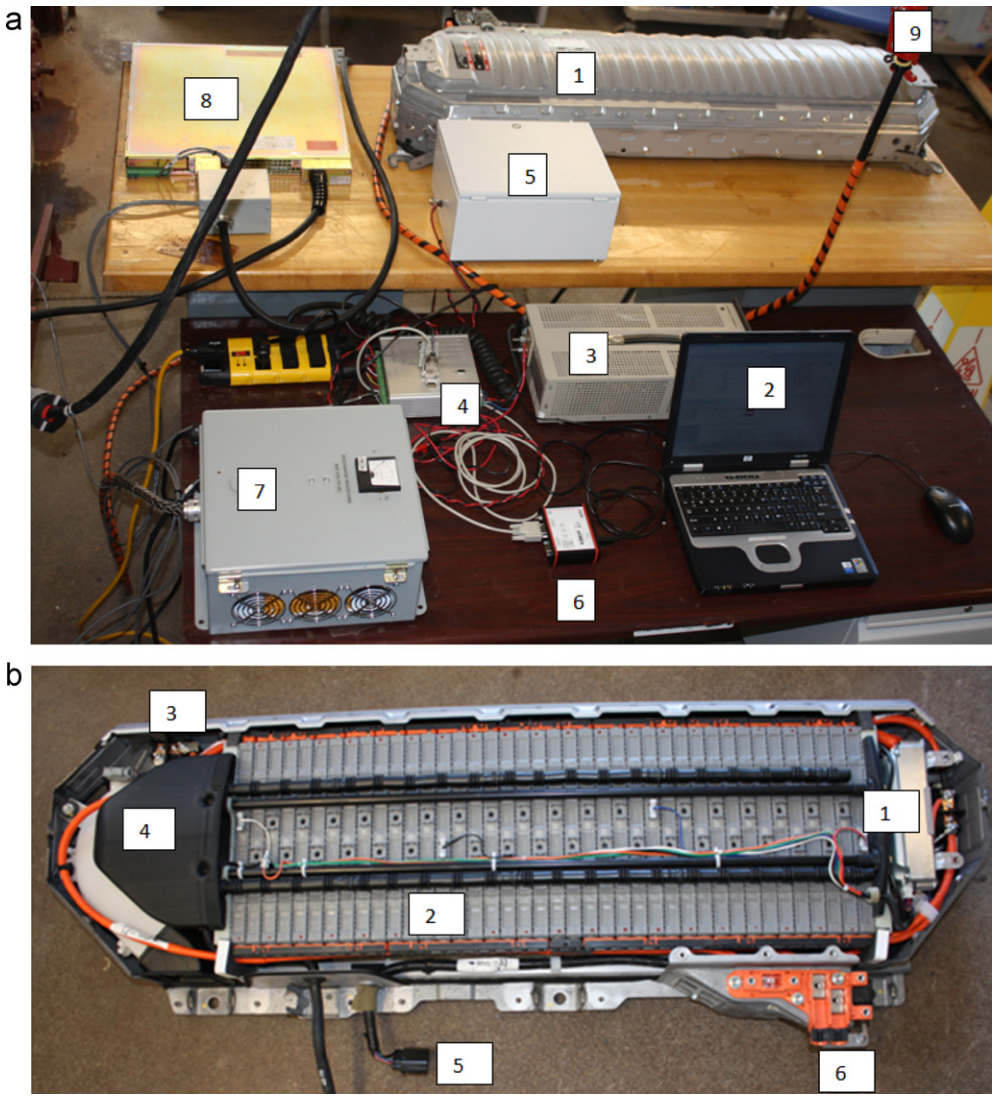

Fig. 3. Pictures of (a) NiMH battery. 1, computer for communicating with the battery and recording data, 2; 12 V power supply, 3; relay and signal box, 4; capacitive load, 5; CANcase XL, 6; resistive load, 7; DC power supply, 8; PV power from array to battery terminals, 9; (b) NiMH battery with the cover removed exposing internal components labeled as follows: BPCM, 1; prismatic battery modules, 2; one of three high voltage relays, 3; fan, 4; 18 pin connector for CAN communication, 5; high-voltage output terminals, 6.

2.6. Resistive load bank for battery discharging

A resistive load bank was designed to discharge the battery at a current of about 2 A, which is approximately a *C*/3 rate. Since the nominal battery voltage was 300 V, and the charge capacity was 6.5 Ah, a resistance of approximately 150 ohms was needed. Three 470 ohm, 300 W Arcol oil-filled resistors (Mouser Electronics, Mansfield, TX) were connected in parallel to make a 157-ohm load bank capable of dissipating 900 W of power. The power resistors were mounted in a box (see Fig. 3a) with three cooling fans to cool the resistors by circulating room air over them. The load bank was equipped with a current shunt to measure the current using LABview.

Table 3
Measurements and calculations of the battery discharging parameters for four discharge tests in which the battery was fully charged prior to the discharge.

Parameter	Test 1	Test 2	Test 3	Test 4
Duration of experiment, min	132.7	123.3	131.2	124.9
Battery maximum module temperature, °C	27.0	21.0	26.0	25.0
Starting battery voltage, V	335	333	335	335
Ending battery voltage, V	254	252	254	254
Minimum module voltage, V	12	12	12	12
Avg. battery discharging current, A	1.90	1.88	1.90	1.91
Avg. *C*-rate, battery discharge	0.293	0.289	0.293	0.295
Avg. battery discharging power, W	586	567	586	592
Energy removed from battery, kWh	1.295	1.167	1.281	1.232
Charge removed from battery, Ah	4.21	3.86	4.17	3.99

2.7. Ametek power supply charging

We utilized a DC power supply to charge the battery at a constant current for comparison to PV charging of the battery. The power supply was an Ametek/Sorenson (San Diego, CA) XFR 600-2 DC power supply (1200 W maximum output). This power supply is capable of outputting from 0 to 600 V and 0–2 A in constant current or constant voltage modes. The power supply had low voltage outputs, proportional to the output voltage and current, that were connected to our National Instruments (Austin, TX) LABview data system to record the power supply output when charging the battery. For battery charging the output voltage was set to 350 V without the battery load attached, i.e., while the battery contactors were open. Then the current output on the power supply was set at approximately 2 A in constant current mode. Next, the battery contactors were closed and the battery was charged from a fully discharged state to a fully charged state (Table 2) at a constant current of approximately 2 A.

2.8. Data acquisition

Details on the data acquisition system and calibrations are described in our earlier report [13]. In brief, two data acquisition systems were used to collect the data from the solar and battery systems. One data acquisition system, LABview, was used to collect data from the solar arrays (voltage, current, solar irradiance and solar array temperature). A second data acquisition system that was slightly different than that used in our earlier battery charging study was used to collect data from the PEVE battery (as well as to wake up the battery, close the battery contactors, and control the BPCM, as discussed earlier). This system consisted of CANcaseXL, V2.0 from Vector CANtech, Inc., with an internal CAN piggy 1050 mag cable installed. This hardware was connected to the USB port on a Hewlett Packard Laptop computer. A cable connected the CANcaseXL to the 18-pin connector on the PEVE battery. The variables from the battery were obtained from the BPCM and were obtained from the CAN bus exiting the battery via the 18-pin connector. The variables included pack voltage, pack current, maximum 2-module voltage, minimum 2-module voltage, maximum 2-module temperature, and minimum 2-module temperature. The internal sensors in the battery pack and the CAN bus, along with the data logging features in CANalyzer were used to record the instantaneous values for these parameters once per second. The LABview system recorded the solar variables once per second, and the two computer clocks were synchronized to the nearest second. This allowed the two data sets to be merged to create the overall data bases for analysis of the response of the battery to the solar energy and solar PV electrical power used to charge the battery. The data was exported from CANalyzer to a comma-delimited data set and read into SAS (Cary, NC) for analysis. The LABview data for both charging and discharging experiments was also read into SAS and combined with the CANalyzer data for analysis.

2.9. Calculation of the PV maximum power point voltage, maximum power, and maximum efficiency

A regression model that predicts the PV maximum power point voltage, current, power, and solar to electrical efficiency as a function of the solar irradiance and PV module temperature was used to predict those quantities in this study. The model derivation is described elsewhere [10]. Briefly, the regression model was a fit to a matrix of predicted values for V_{mpp} and I_{mpp} for Sanyo PV modules that were based on long-term measurements performed by Sandia National Laboratories. The model allows us to calculate the maximum power-point (MPP) values for the voltage (V_{mpp}), the current (I_{mpp}), and the power ($P_{max} = V_{mpp} \times I_{mpp}$), and the PV solar to electrical efficiency (maximum PV efficiency = 100% × P_{max}/total solar energy incident on the PV modules). These maximum PV output predictions were compared the actual PV system efficiency when it was connected to the battery load to determine the coupling factor between the PV and battery systems and to understand how close to the MPP the battery load was charged.

3. Results and discussion

3.1. Battery pack and solar measurements and calculations

3.1.1. Computations of battery pack changes in electrical energy and charge

The energy added to or removed from the battery pack (ΔE) during the 1 s data collection time intervals (Δt) in our experiments was calculated from the battery voltage (V_{batt}) and current (I_{batt}) according to Eq. (1):

$$\Delta E \text{ battery pack, Wh} = V_{batt} \times I_{batt} \times (\Delta t/3600) \quad (1)$$

The total energy added to the battery over a charging or discharging experiment was calculated by summing the individual ΔE values over the experimental run. Note that Δt/3600 has units of *h*.

The charge that was added (or subtracted in discharging experiments) in Ah was computed in a like manner from the charge added over a 1-s interval:

$$\Delta Q, \text{ Ah} = I_{batt} \times (\Delta t/3600) \quad (2)$$

Summing ΔQ over a charging or discharging experiment to get the total charge added in Ah.

The charging and discharging experiments covered an operational range between a fully discharged and a fully charged state for the battery as defined by the voltage limits used in Table 2.

3.1.2. Solar energy and solar electrical measurements during battery charging

The solar energy incident on the solar modules over the 1 s time interval Δt was derived by measuring the solar irradiance (W m^{-2}) with the LI-COR radiometer, and computing the energy incident on the number of modules used (from five to eight). The formula was:

$$\Delta E \text{ solar energy, Wh} = \text{Solar irradiance, W m}^{-2} \times 1.179\,\text{m}^2 \times \text{modules} \times (\Delta t/3600) \quad (3)$$

The ΔE values in Eq. (3) were summed over the time interval for the battery charging experiment to obtain the total solar energy incident on the solar PV modules used in the test.

The solar electrical energy was computed from the average voltage and current measured for the high-voltage array, V_{solar} and I_{solar}, respectively, over the 1-s interval Δt.

$$\Delta E \text{ solar PV electrical energy, Wh} = V_{solar} \times I_{solar} \times (\Delta t/3600) \quad (4)$$

The total solar PV electrical energy generated over an experiment was the sum of the solar PV electrical energy, ΔE in Eq. (4), over the course of a battery charging experiment. Note that V_{solar} and V_{batt} can differ slightly because there are some losses in the cables and connectors connecting the PV and battery systems. However, I_{solar} and I_{batt} are the same because all of the solar current is delivered to the battery.

3.1.3. Solar energy and solar PV electrical energy to battery charge efficiency calculations

We can compute the PV efficiency from the solar PV electrical energy in Eq. (4) divided by the total solar energy incident on the PV modules in Eq. (3):

$$\text{PV solar electrical efficiency, \%} = 100\% \times \frac{\Delta E\ \text{PV electrical solar energy, Wh}}{\Delta E\ \text{solar energy, Wh}} \quad (5)$$

Second, the solar system to battery charging efficiency was computed as the electrical energy added to the battery pack, Eq. (1), divided by the solar energy incident on the PV modules, Eq. (3):

$$\text{Solar energy to battery charging efficiency, \%} = 100\% \times \frac{\Delta E\ \text{battery pack, Wh}}{\Delta E\ \text{solar energy, Wh}} \quad (6)$$

In our study there is a direct connection between the PV and battery systems with no intervening power electronics (DC–DC converters) so nearly all of the PV energy (minus very small copper losses) was delivered to the battery, so no accounting for losses in power conversion are needed in contrast to our earlier study [13]. However, the PV system does not necessarily deliver the maximum electrical energy to the battery, because the battery, depending on its nominal voltage and state of charge, pulls the PV system to its terminal voltage, which may not be the PV MPP. In order to characterize how much of its potential electrical power the PV system delivers to the battery in a test, we can define a coupling factor as the ratio of the PV electrical power when the PV system is connected to the battery load divided by the maximum PV power:

$$\text{Coupling factor} = \frac{\text{PV power achieved, W}}{\text{Maximum PV power, W}} \quad (7)$$

In Eq. (7), the PV power achieved is the measured solar voltage, V_{solar}, times the measured solar current I_{solar} and the maximum power, P_{max}, is the power produced at the PV MPP. We can calculate the P_{max} utilizing the PV regression model developed in our earlier work [10]. In that earlier work we utilized the following: (1) V_{mpp} is a logarithmic function of irradiance and a linear function of temperature, and (2) I_{mpp} is a linear function of irradiance and a linear function of temperature. The resulting models were:

$$V_{mpp}, \text{V} = 9.85 - (0.1683 \times T_{array}) + (14.45 \times \ln(\text{irradiance})) - (1.06044 \times \ln^2(\text{irradiance})) \quad (8)$$

where T_{array} has units of °C and irradiance is the solar irradiance with units of W m^{-2}.

$$I_{mpp}, \text{A} = -0.00509 - (0.0002175 \times T_{array}) + (0.00348 \times \text{irradiance}) \quad (9)$$

P_{max} was calculated from $V_{mpp} \times I_{mpp}$

$$P_{max}, \text{W} = V_{mpp} \times I_{mpp} \quad (10)$$

For example, if six PV modules were used (area = 7.07 m^2), the module temperature (T_{array}) during a test was 25 °C, and the solar irradiance was 1000 W m^{-2}, then P_{max} would be 1140 W and the maximum PV efficiency would be 16.1%. This prediction is identical to the values at STC conditions, Table 1, taken from the PV manufacturer's data sheet [20].

Because the battery terminal voltage changes during charging, even if the PV system were well coupled at the beginning of a test it would not necessarily remain well coupled in a steady state throughout the test. Therefore, the battery characteristics, particularly the range of voltages at the battery terminals during charging and the time spent at the voltages within that range, will be an important factor in determining the PV battery charging efficiency.

3.2. Battery pack discharging experiments

Prior to the solar charging experiments, the battery was discharged until the contactors opened due to one of the constraints regarding the minimum 2-module block voltage or the minimum pack voltage in Table 2. The results for four discharging experiments conducted with one battery pack are listed in Table 3. An examination of the results shows that a substantial portion of the nominal battery energy and charge values for the NiMH battery (energy = 1.8 kWh, charge = 6.5 Ah) was removed with our discharging protocol. An inspection of the data in Table 3 reveals that up to 1.4 kWh of energy and 4.6 Ah of charge was removed in a discharging experiment. After a discharge experiment, the battery open-circuit voltage recovered to higher values, but this was just a "surface" charge. For example, when a second discharge experiment was run on a previously discharged battery, only about ~20 Wh of additional energy, and ~0.1 Ah of charge were removed (this is discussed in more detail later).

A plot of the voltage and current versus time is shown in Fig. 4a for Test 4 in Table 3. The battery voltage decreased from 335 V to 254 V over the 125-min experiment. The current decreased from 2.1 A to 1.57 A over the experiment, resulting in a decrease in the discharge power from an initial value of approximately 700 W to a final value of 399 W. Fig. 4b shows the charge removal from the battery versus the battery voltage during the whole discharge test. In this experiment approximately 4.0 Ah of charge was removed from the battery (Table 3). The discharge rate as a function of voltage shown in Fig. 4b was initially low, followed by a period of increased charge removal, and finally period of slower charge removal. Most of the charge removal occurs between battery voltages of 290 and 310 V. In this test, approximately 1.23 kWh of energy was removed from the battery (Table 3). This experiment was terminated when one of the battery 2-module voltages fell below 12 V (one of the criteria in Table 2), so the battery pack voltage did not attain its lowest possible value of 240 V.

The average energy removed in the four tests was 1.243 kWh and the average charge removed was 4.06 Ah. The coefficient of variation for the energy and charge removed was less than 5%. There was also very good consistency in the starting and ending voltages from Test 1 to Test 4.

3.3. Battery pack charging experiments

3.3.1. Solar-powered high-voltage battery charging system capabilities

The output of the system of five, six, seven, or eight modules in series was modeled using a fit to a current–voltage (I–V) curve for the Sanyo modules obtained on a sunny day using a resistive load bank [7]. An example of such an I–V curve will be given later. This I–V curve can be used to understand how the different outputs can interrogate the battery charging curve for the NiMH battery. From those results, the PV open circuit voltage, V_{oc}, the maximum power point voltage, V_{mpp}, and the voltages where the PV system electrical power output is 90% of the maximum power output, $V_{90}(L)$ and $V_{90}(H)$, were estimated for sets of five, six, and eight modules in series and the results are tabulated in Table 4. One column also shows the maximum battery voltage attained, 340 V, divided by the MPP voltage, V_{mpp}. The values for V_{oc} and V_{mpp} in Table 4 are slightly different than those in Table 1 because of the higher system temperature and the negative temperature coefficient of the PV output voltage as a function of temperature.

Although the values in Table 4 will vary with the solar conditions (solar irradiance and module temperature), they can be used to illustrate how the high-voltage array with variable voltage outputs can be used to determine an optimal charging system for the NiMH battery using series-combinations of Sanyo HIP190-BA3 modules.

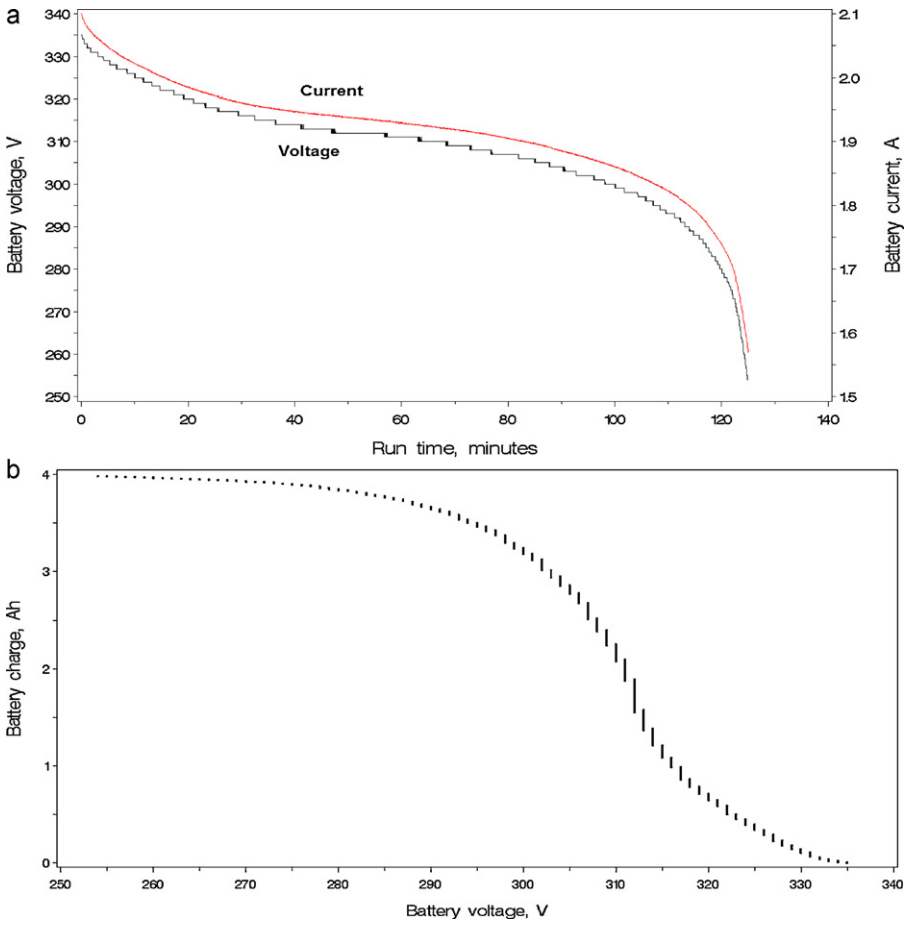

Fig. 4. Results of a battery discharging test (Test 4, Table 3) for an initially fully charged battery: (a) battery voltage and current versus time, and (b) battery charge versus battery voltage.

Clearly the series combination using five modules is incapable of charging the battery fully as V_{oc} < 340 V. All of the other combinations can charge the battery to its full potential and we will now discuss the results.

3.3.2. *Tests with the number of modules in series constant throughout a charging test*

A total of five battery tests were conducted during the summer and fall of 2010 in which the number of solar modules in series was fixed at six, seven, or eight and the battery was charged from its minimum state, obtained by fully discharging it, to its maximum charge state, based on the criteria for a fully discharged and a fully charged battery in Table 2. Five modules could not charge the battery to the final state of 340 V, so results using five modules in series are discussed later in this report.

The results of the experiments are shown in Table 5. The experiments lasted from about an hour to about two and one-half hours. Solar charging added from 1.23 to 1.72 kWh of energy to the battery and 3.66 to 5.21 Ah of charge. This is a significant fraction of the nominal battery capacity of 1.8 kWh and 6.5 Ah. For example, these charging experiments added up to 80% of the battery charge capacity. The beginning battery voltage was typically 275–285 V and the ending battery voltage was always 340 V. Charging with six modules in series kept the PV system above the PV MPP for most of the experiment, while charging with seven or eight modules in series kept the PV system below the PV MPP over the whole experiment. The small change in the maximum battery temperature, from 25 °C to 29 °C, probably reflects the higher room temperature on hot, summer days.

In two tests with six modules in series the average solar to battery charge efficiency over the whole test was 12.2% and 13.3%, and

Table 4
Solar array voltage parameters for various series strings of Sanyo HIP-190BA3 modules based on a PV *I–V* curve measured on a sunny day.[a]

Number of modules in series	V_{oc}	V_{mpp}	V_{batt}/V_{mpp}[b]	$V_{90}(L)$[c]	$V_{90}(H)$[c]
5	322	249	1.37	210	276
6	386	299	1.14	251	331
7	451	349	0.98	293	386
8	515	398	0.85	335	442

[a] Module temperature of 45 °C and a solar irradiance of 1050 W m^{-2}.
[b] The battery terminal cut-off voltage for charging the Panasonic NiMH battery is 340 V (highest V_{batt} = 340 V), Table 2.
[c] $V_{90}(L)$ is the lower voltage (less than V_{mpp}) where 90% of the PV maximum power, P_{max} is produced and $V_{90}(H)$ is the higher voltage (greater than V_{mpp}) where 90% of P_{max} is produced.

Table 5
Measurements and calculations of the PV and battery charging parameters during five tests in which the number of modules in series was constant for the whole charging experiment.

Parameter	Test date				
	8/17	8/27	9/29	11/11	10/6
Number of modules in series	6	6	7	7	8
Duration of experiment, min	151.4	125.8	64.7	122.5	95.1
Avg. solar irradiance, W m^{-2}	707	972	930	642	720
Avg. PV module temperature, °C	45.7	54.2	45.2	37.9	36.9
Avg. PV voltage, V	334.6	332.8	336.2	335.7	335.0
Avg. PV current, A	2.0	2.6	3.4	2.3	2.7
Avg. PV power, W	668	854	1154	783	905
Total PV electrical energy, kWh	1.69	1.77	1.24	1.60	1.43
PV V_{mpp}[a], V	306.4	299.5	360.1	367.4	420.2
PV, V_{oc}, V	376.0	374.0	446.5	447.6	513.9
Avg. PV voltage, V_{mpp}	1.09	1.11	0.93	0.91	0.80
Solar energy input, kWh	12.64	14.42	8.28	10.82	10.78
Solar to electric efficiency, %	13.3	12.3	15.0	14.8	13.3
Max. solar PV to electrical efficiency[a]	15.0	14.7	15.1	15.4	15.4
Coupling factor	0.89	0.84	0.99	0.96	0.86
Battery maximum module temperature, °C	29	27	24	25	25
Starting battery voltage, V	285	278	275	281	285
Ending battery voltage, V	340	340	340	340	340
Avg. battery voltage, V	333	331	335	334	334
Avg. battery charging current, A	2.0	2.5	3.4	2.3	2.7
Avg. battery charge, *C*-rate[b]	0.31	0.38	0.52	0.36	0.42
Avg. battery charging power, W	666	821	1137	776	907
Energy added to battery, kWh	1.68	1.72	1.23	1.58	1.44
Charge added to battery, Ah	5.05	5.21	3.66	4.75	4.32
Solar to battery charge efficiency, %	13.3	12.2	15.0	14.7	13.3

[a] These values were calculated using the PV model derived in earlier work [10] and expressed in Eqs. (8)–(10).
[b] The *C*-rate is the discharging current divided by the Ah capacity of the battery (6.5 Ah for the battery tested in our study).

the coupling factor was 0.84 and 0.89, respectively. As shown in Table 1, under STC six modules in series has a sufficient V_{oc} to charge the battery to 340 V, but this voltage is past V_{mpp}, so the efficiency is falling with time throughout the experiment. For two experiments conducted with seven modules in series, the solar to battery charge efficiency was 14.7% and 15.0%, with coupling factors of 0.96 and 0.99, respectively. The seven-module series combination was the most efficient in charging the battery. For eight modules in series, the solar to battery charging efficiency was 13.3% and the coupling factor was 0.86.

Fig. 5 shows an example of the results form a solar battery charging test in which seven modules in series was tested. Fig. 5a shows the battery voltage and current and Fig. 5b shows the solar to battery charging efficiency. This was a sunny day with very constant solar irradiance so the battery charging current was relatively constant at about 3.3 A. The battery voltage quickly increased from an initial value of 275 V to 330 V in about 7 min. It took approximately another hour to reach 340 V, at which point the contactors opened and the experiment was terminated. The solar to battery charging efficiency, shown in Fig. 5b, increased during the initial few minutes of the experiment, and then remained relatively constant throughout the test.

Fig. 6 shows the results from the test in which eight modules in series were used to charge the battery. Initially, it was very sunny at the beginning of this test. The initial battery voltage at the start of the test was 285 V and it quickly increased to about 320 V about 5 min into the experiment. The charging current was nearly constant at 3.5 A (this is full output for the solar modules under bright sunshine). At about 40 min into the experiment, clouds moved in and there was an initial enhancement in the power output of the solar system, followed by a decrease in output as it became cloudy and there was no further direct sunshine. Notice the choppy behavior in the battery charging current in Fig. 6a. However, it is interesting that the solar to battery charging efficiency was little affected by the clouds, increasing slightly during the cloudy period as shown in Fig. 6b. The experiment was terminated after about 95 min of charging as the battery voltage reached 340 V and the contactors opened.

Fig. 7 shows sample PV *I*–*V* and power–*V* curves representing the PV system characteristics on a sunny day, together with the battery *I*–*V* combinations for a charging experiment with seven modules in series (the optimal number with our PV system for this battery). The PV *I*–*V* data has been discussed elsewhere [7] and was obtained for a set of PV modules wired in parallel. This single-module data has been multiplied by seven to represent a seven-module in series combination for Fig. 7. The battery charging data is shown as a red series of data points. For this data, time was increasing for the data points moving from left to right. Using this single snapshot of the PV system characteristics helps to understand the dynamics of the coupled PV-battery system during charging. The battery load initially pulls the PV power away from the MPP voltage and the PV power delivered to the battery is decreased. However, as the battery charges, the PV power and charge delivered to the battery is increased as the system nears the MPP.

Fig. 7 also illustrates another important point about solar PV battery charging. To the left of the maximum power point, the slope of the power–*V* curve is relatively constant and is about 4 W V^{-1}. That is, each volt of movement to the left, away from the MPP reduces the power by about 4 W. However, far to the right of the maximum power point, near the open circuit voltage, the slope of the power–*V* curve is approximately 23 W V^{-1}, so the power penalty is much greater in moving to the right, away from the MPP, especially as we get nearer to V_{oc}. Thus, it is very important to design a PV battery charging system such that the battery voltage at full charge is not too far past the MPP, i.e., such that it never reaches V_{oc}, because at V_{oc} the solar to battery charging efficiency becomes zero. A good rule of thumb is that the PV system $V_{90}(H)$ should be equal to or greater than the battery full charge voltage.

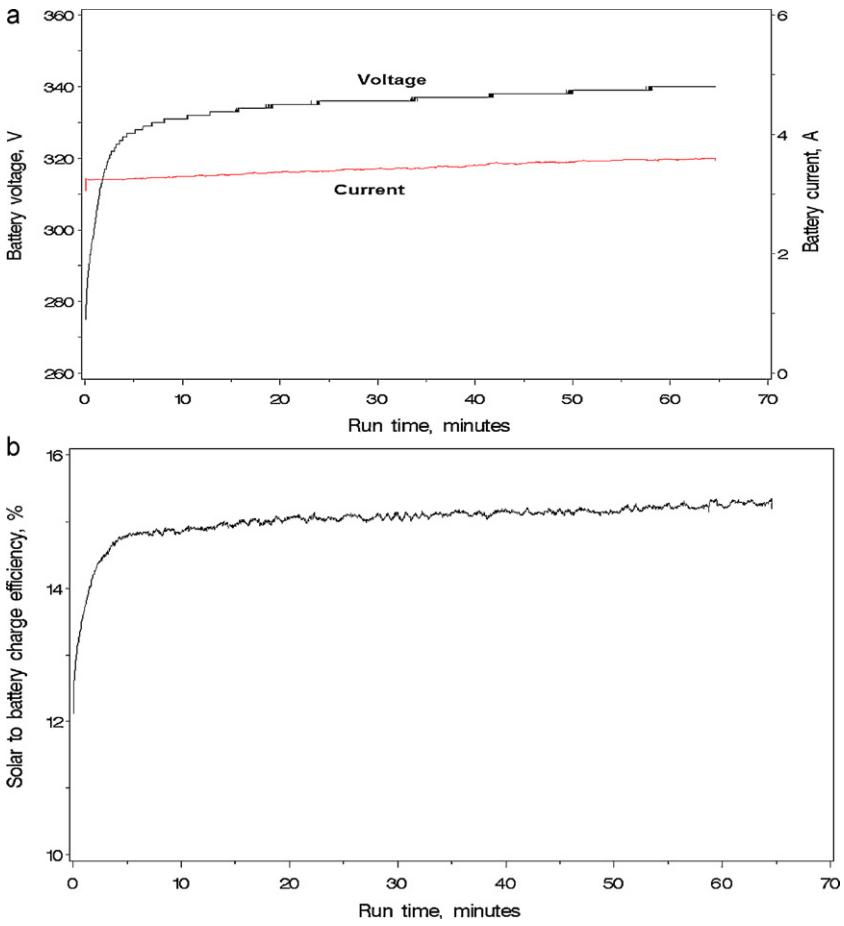

Fig. 5. Results for the battery test on September 29, 2010 in which seven modules in series were used to charge the NiMH battery from a fully discharged state to a fully charged state as defined by Table 2: (a) battery voltage and current, and (b) solar to battery charge efficiency.

3.3.3. Tests in which the number of modules in series was varied from five to eight on a given day

A very illustrative test was possible with the variable high-voltage array constructed in this study. On a sunny day with no cloudy periods we varied the number of modules in series over the possible range from five to eight over short periods of about 10 min. This test was performed on three different days. Fig. 8 shows the results for 1-s data points for the combined data set of all three days. The data from the different days fit together nicely and form a curve of efficiency versus the ratio of the charging voltage divided by the maximum power point voltage. In general, for sets of points with the same number of modules in series, the data points have a temporal pattern of moving from left to right. For example, for five modules in series, the first data points that were obtained for a discharged battery at the lowest voltage, and thus the lowest V_{solar}/V_{mpp} in Fig. 8, had a solar to battery charging efficiency of up to 10%. Then, as the battery terminal voltage increased as the battery gained charge and V_{solar}/V_{mpp} increased, the solar to battery charge efficiency decreased, eventually approaching zero for the five-module combination. On the other hand for strings of seven modules in series, the efficiency was increasing as the battery became charged and the battery terminal voltage increased. The maximum power point voltage was calculated from the solar irradiance and module temperature, as described earlier. Notice in particular that the solar to battery charge efficiency is maximized at a value of about 15% near the ratio of unity, as expected. Also notice that a string of five modules in series formed a self-regulating system, in that it could not overcharge the battery. Notice how the results in Fig. 8 interrogated the PV battery charging curve over the complete range of V_{batt}/V_{mpp} shown in Table 4.

3.3.4. Battery charging using a DC power supply

Four experiments were conducted in which a discharged battery was fully charged using the Ametek DC power supply. Table 6 shows a summary of the results of these experiments. The power supply charged the battery at a very constant current and *C*-rate over the whole experiment that typically took about 140 min. The battery voltage increased from starting values of about 280 V to the full-charge value of 340 V. The maximum battery temperature was consistent between the four tests that were all conducted on cool days where the room temperature in the laboratory was maintained at about 20 °C. The energy and charge added to the battery averaged 1.57 and 4.8 Ah, respectively, with a coefficient of variation of only 3% over the four tests.

3.3.5. Frequency distributions of the battery voltage when charging using PV solar, a power supply, or discharging using a resistive load bank

Fig. 9 shows a comparison of the frequency distributions for the battery voltage during two types of charging experiments as well as a discharging experiment. For the charging experiment data we utilized the September 29 experiment with seven modules in series from Table 5 and Test 4 from the Ametek charging experiments in Table 6. The discharging experiment was from Test 4 in Table 3. For the solar PV charging the battery voltage frequency distribution, Fig. 9a, was heavily skewed toward the higher voltages, i.e., over 75% of the time the battery voltage was over 338 V. This is

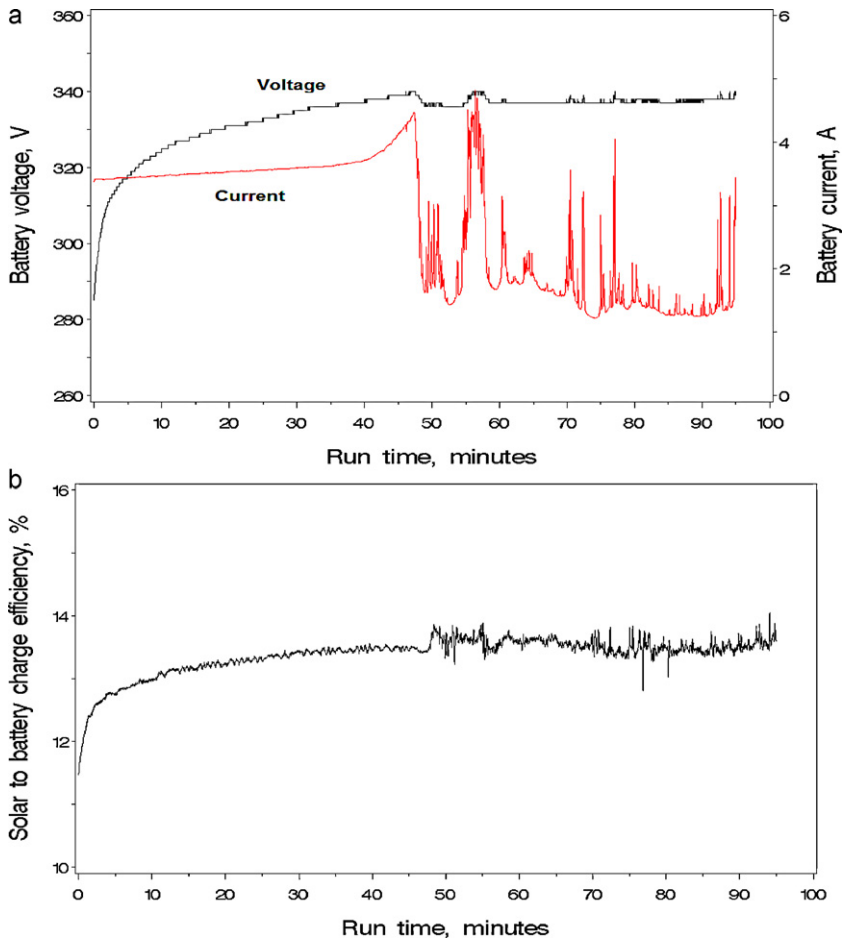

Fig. 6. Results for the battery test on October 6, 2010 in which eight modules in series were used to charge the NiMH battery from a fully discharged state to a fully charged state as defined by Table 2: (a) battery voltage and current, and (b) solar to battery charge efficiency.

important because the PV charging efficiency is strongly affected by PV system operating voltage, which in turn is determined by the battery charging voltage because the battery load pulls the PV system to its terminal voltage. The battery charging current was very constant for this test (see Fig. 5a), so over 75% of the energy and charge was also added to the battery at the higher voltages. From Table 5, the PV MPP was approximately 360 V for this experiment resulting in a high coupling factor between the PV and battery systems for most of the experiment (0.99) and a solar to battery charge efficiency of 15%.

The battery charging voltage frequency distribution using constant-current charging from the Ametek power supply, Fig. 9b, is also skewed toward the higher voltages, although it is quite not as skewed as the solar PV charging frequency distribution shown in Fig. 9a. For the power supply charging over 75% of the time the battery voltage was over 334 V. In general, the battery charging frequency distributions for the solar-PV and power-supply charging are similar.

In contrast, for battery discharging, the battery voltage moved more evenly across the range of values from high voltages to low voltages, although there was slight skewing toward the higher voltages. This data also illustrates that the battery pack voltage did not attain the lowest possible value of 240 V prior to termination of the test due to attaining one of the limits in Table 2. Rather, for this and all other battery discharging tests the discharge was terminated when one of the 2-module block voltages reached 12 V. When the pack was new and the blocks were more balanced [13] the pack voltage more closely approached 240 V upon full discharge.

Table 6
Measurements and calculations of the battery charging parameters for four charge tests using an Ametek DC power supply.

Parameter	Test 1	Test 2	Test 3	Test 4
Duration of experiment, min	140.2	144.1	138.1	133.2
Battery maximum module temperature, °C	25	25	25	25
Starting battery voltage, V	287	280	276	277
Ending battery voltage, V	340	340	340	340
Maximum module voltage, V	17	17	17	17
Avg. battery charging current, A	2.08	2.08	2.08	2.07
Avg. battery charge, *C*-rate[a]	0.319	0.319	0.319	0.319
Avg. battery charging power, W	677	676	684	679
Energy added to battery, kWh	1.583	1.623	1.575	1.506
Charge added to battery, Ah	4.85	4.98	4.78	4.61

[a] The *C*-rate is the charging current divided by the Ah capacity of the battery (6.5 Ah for the battery tested in our study).

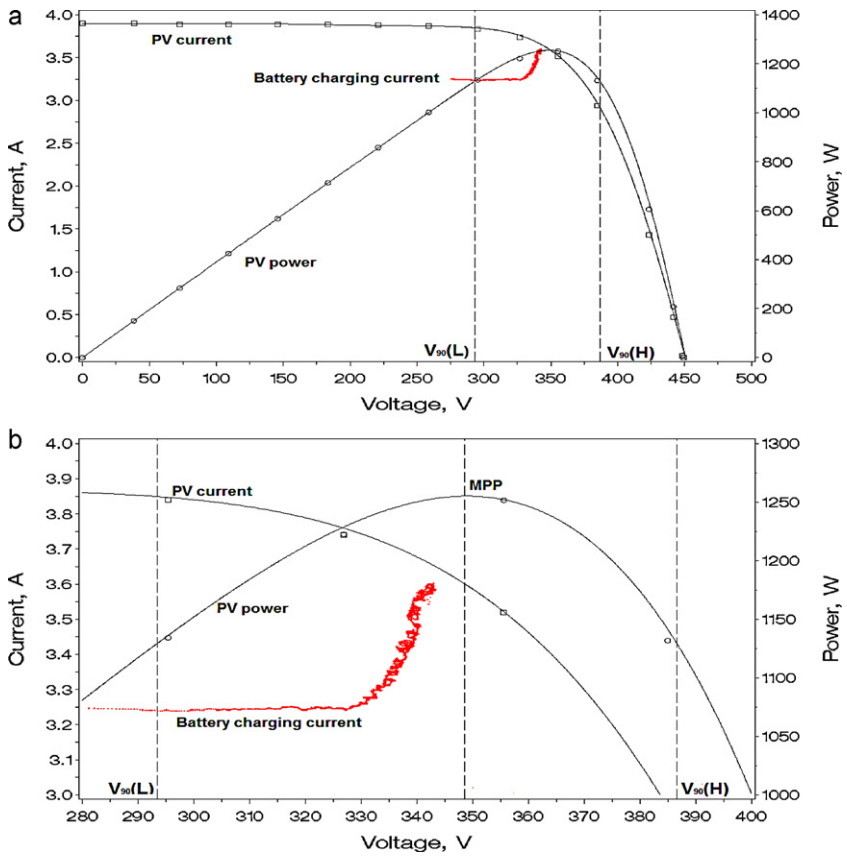

Fig. 7. Plots of: (a) PV current–voltage (I–V) and PV power–voltage curves for seven modules in series measured on a sunny day along with battery charging I–V data points from the September 29, 2010 experiment (Table 5), and (b) the same data with an expanded view of the region between $V_{90}(L)$ and $V_{90}(H)$.

3.3.6. Comparison of charge removed via discharging and added via charging

The energy efficiency of a battery is the ratio of the power it can deliver when connected to a load divided by the power it takes to charge it. Generally, any loss in efficiency is due to higher voltage during the charging process than during the discharging process for a given change in the battery state of charge. Most commercial rechargeable batteries have long cycle lives so the coulombic efficiency (the ratio of the charge removed over the charge added) is near unity.

However, our experiments, utilizing the simple "voltage under load" protocol in Table 2, do not necessarily charge and discharge the battery consistently between two stable state of charge points (as discussed in the next section), although our protocol is useful as a proof of concept for efficient solar charging of high-voltage traction batteries. From the data in Tables 4 and 5, the ratio of the charge

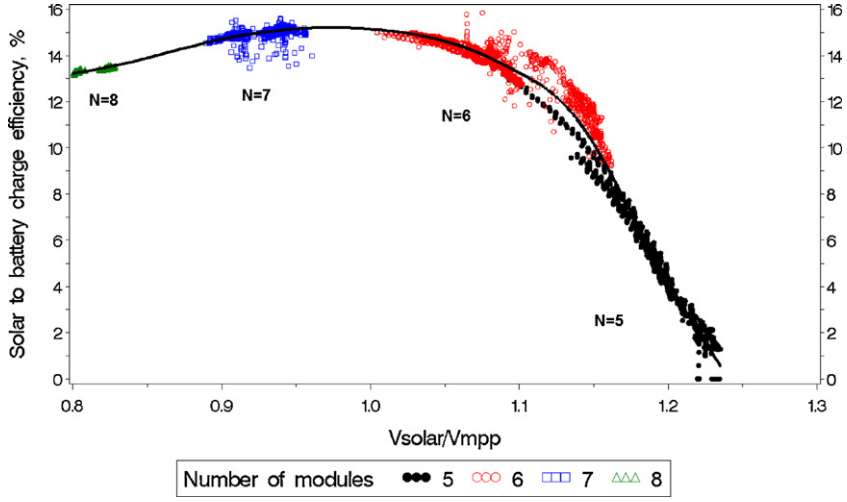

Fig. 8. Plot of the solar to battery charge efficiency as a function of the ratio of solar battery charging voltage divided by the PV maximum power point voltage. In these experiments the number of PV modules in series was varied over the range from five to eight over short intervals on the same day with nearly constant solar irradiance and module temperature over the short interval. The experiments were conducted on three different days (September 13, September 29, and November 11, 2010) and the data from those days was combined to make the figure. The spline fit (solid black line) was drawn to fit all of the data.

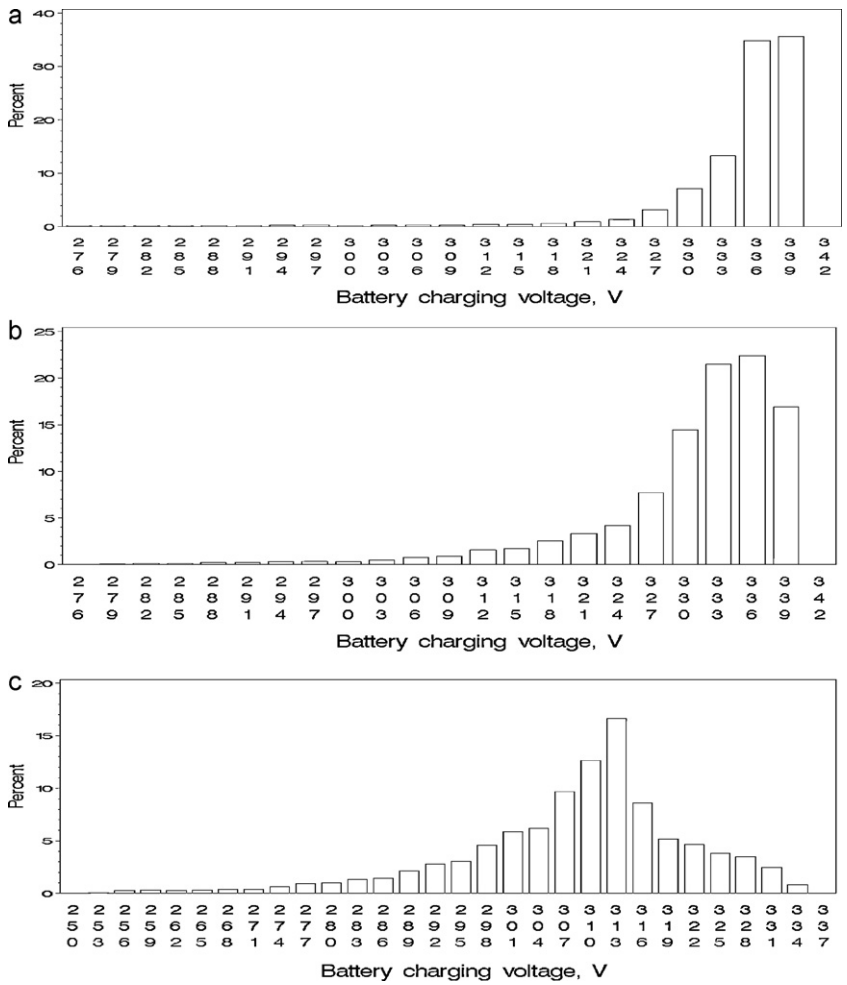

Fig. 9. Frequency distributions of the battery voltage for: (a) PV solar charging with seven modules in series, (b) charging with the Ametek power supply, and (c) discharging with the resistive load bank.

removed during discharging to the charge added during charging is 0.84. The charging seemed to be more equalized over the 20 2-module blocks so that charging termination occurred because the battery pack voltage exceeded 340 V. On the other hand, the discharging was most often terminated by the criterion where one 2-module block voltage fell below 12 V, which resulted in less charge removed from the battery than if the pack had reached 240 V. In normal use in a hybrid vehicle this imbalance is probably not important as the battery state of charge does not undergo such large swings in discharging and charging. That is, the battery is not discharged for a long period (hours) before it begins receiving some charge. However, this could be more important for a plug-in hybrid where the battery may be fully discharged and then charged overnight. A difference in the charging and discharging behavior for this battery is consistent with the hysteresis in the voltage/state of charge behavior in the NiMH system [23–27].

3.3.7. *Battery pack open-circuit voltage following a discharge or charge experiment*

In preparation for charging, the battery was typically discharged to a pack voltage of approximately 250 V as shown in Fig. 4a (this voltage corresponded at one block voltage reaching a 12 V minimum). However, in the time between the discharge and the solar charging, the battery open-circuit voltage was observed to recover by approximately 30 V. For example, in Fig. 6a, the starting battery voltage was 282 V, although the ending voltage on discharge was 252 V. A small decrease in the battery pack open circuit voltage was observed following charging, e.g., the initial voltage was 340 V at the termination of a charging experiment and the open circuit voltage decreased to 331 V over about a 3 h period. Thus, the increase in the open circuit voltage following a discharge experiment (~30 V) was much greater than the decrease in the open circuit voltage (~10 V) following a charging experiment.

These observed changes in the NiMH open-circuit voltage can explain why the energy and charge removed in discharge experiments (Table 3) does not equal the energy and charge added in the charging experiments (Tables 5 and 6). We discharged and charged the battery to set voltages (Table 2) under load or while connected to a charging system, but the battery state of charge is more related to the battery open-circuit voltage after a rest period. If we wanted to use our NiMH battery for solar energy storage in a practical system, as opposed to the proof of concept we have described, we would need a more complex algorithm to control the discharging/charging of the battery, such as those discussed elsewhere [23–27].

3.4. *Comparison to previous work*

In our earlier work we used our 50 V solar PV system to directly charge small strings of A123 Li-ion batteries [12], as well as to charge the same NiMH PEVE battery as was used in the present study by using a DC-DC converter to boost the low 50 V system voltages to 350 V [13]. In the low-voltage Li-ion battery charging, a solar to battery charge efficiency of 14.5% was attained for an

optimal coupling between the solar PV and battery systems. In our earlier high-voltage battery charging work, the best efficiency we recorded for a complete battery charging test was 13.5%. Eliminating the DC–DC converter, and optimizing the coupling between the PV and battery systems in this work, we achieved a 15.0% solar to battery charging efficiency. Losses in the coupling between the PV and battery system were negligible in the present study. This study serves as a proof of concept for an optimized direct DC high voltage PV battery charging system and as the basis for a PV system capable of directly charging a range of high-voltage traction batteries.

4. Summary

We designed and tested a PV solar battery charging system consisting of a variable number of 50 V solar modules in series ranging from five to eight modules. This novel PV testing system was used to charge the NiMH battery used in the GM 2-mode hybrid over a range of PV system voltages in order to devise an optimal PV-battery charging system. An optimized PV charging system utilized seven 50 V PV modules in series with the battery charging controlled by the internal battery pack control module. This design resulted in a simple system with a high solar to battery charging efficiency by keeping the coupling of the solar energy and battery charging near unity over the whole battery charging curve. The high efficiency of the battery charging makes this a very attractive use of renewable solar energy. The test results prove the concept of direct PV solar DC charging for plug-in electric vehicles, extended range electric vehicles, and battery electric vehicles, and show that an optimized PV system regulated by the internal BPCM can be developed for home or commercial battery charging systems. Because there is no standard voltage for high voltage batteries, PV systems developed to directly charge different electric vehicles will need to have a provision for varying the number of modules in series to accommodate the different charge termination voltages.

This research has also prepared us for the next step in our study of solar battery charging of high-voltage BEV and EREV vehicle batteries—evaluation of direct charging of a Chevrolet Volt battery pack. That will allow testing over a much wider range of energy addition (approximately 10 kWh of usable electrical energy), than was possible with the NiMH battery tested in this study.

5. Conclusions

We designed, built, and tested a high-voltage PV array in which the number of 50 V modules that were wired in series could be varied from five to eight. This variable voltage output was used to directly charge a high-voltage NiMH traction battery with DC electricity. The battery we tested was the same as those used in the GM 2-mode hybrid electric vehicles (Tahoe, Yukon, Escalade, Silverado, and Sierra). Using this system, we measured the solar to battery charging efficiency of the four possible photovoltaic (PV) system voltage outputs over the range from a fully discharged state to a fully charged state for the NiMH battery. The optimal PV charging system had seven PV modules in series and charged the battery with an efficiency as high as 15%. This is higher than the 13.5% efficiency attained in our previous work where DC–DC conversion was used to boost the 50 V module voltages to 350 V.

The measurements using the variable voltage output PV array, along with a model to predict the PV maximum power point voltage as a function of the solar irradiance and PV module temperature, were used to determine the coupling factor, that is, the ratio of the amount of solar energy delivered to the battery load divided by the maximum solar electricity generated by the PV system under the ambient conditions at the time of the experiment. The coupling factor approached unity for the seven-module PV series system.

The solar PV charging system had a charging rate of from 0.31 to 0.52*C* (1*C* rate is 6.5 A charging current for the NiMH battery) depending on how many modules were used, the efficiency of the charging, and the solar irradiance and module temperature. Typically 1.2–1.7 kWh of energy and 3.7–5.2 Ah of charge were added to a discharged battery in a charging experiment. The charging required a period of from 65 to 151 min. For comparison, the nominal energy and charge storage capacities of the NiMH battery are 1.8 kWh and 6.5 Ah, respectively.

The test results prove the concept of direct PV solar charging for plug-in vehicles (extended range electric vehicles) and show that a direct DC system could be used for home or commercial charging systems to deliver over 90% of the solar electric energy produced by the PV system to charging a high-voltage traction battery. Importantly, the battery control system built into the battery pack can be used to regulate the point at which charging is terminated, effectively making it the charge controller. For charging a given high-voltage traction battery, this makes the design of the PV solar system relatively simple. However, because there is no standard voltage for traction batteries, a generalized solar battery charging system would need to have provisions for a variable output voltage, adding or subtracting modules, depending on the traction battery charge-termination voltage point.

Acknowledgements

We wish to acknowledge the valuable help from our General Motors colleagues Carlos Franca and Vance McCabe (site arrangements and maintenance), Douglas Drauch, Morgan Li, Vernon Newhouse (Vector software and battery–computer interface), Morgan Li and Michael W. Rogers (LabView program), Ciro Spigno (battery charging algorithm) and David Ouwerkerk (helpful discussions). Special thanks to, Brian Prokuda (Keweenaw Power Systems, Inc.) and David Mamo (Mattic Electric) for help with the design and building of the high-voltage PV array wiring system.

References

[1] A. Taub, Conference on Electrifying Transportation, Presented at the North Carolina Solar Center, North Carolina State University, May 27, 2009, Available from: http://www.ncsc.ncsu.edu/cleantransportation/docs/Events/2009_5-27_Taub_GM-EV.pdf.
[2] C. Freese, Presentation to the Hydrogen and Fuel Cell Technical Advisory Committee (HTAC), U.S. Department of Energy, Washington, DC, June 3, 2010, Available from: http://www.hydrogen.energy.gov/pdfs/3_freese_0610.pdf.
[3] W.J. Mitchell, C.E. Borroni-Bird, L.D. Burns, Reinventing the Automobile: Personal Urban Mobility for the 21st Century, MIT Press, Cambridge, MA, 2010.
[4] L.D. Burns, J.B. McCormick, C.E. Borroni-Bird, Scientific American 287 (2002) 64–73.
[5] E.D. Tate, M.O. Harpster, P.J. Savagian, SAE paper 2009-01-0458.
[6] L. Edsall, Chevrolet Volt: Charging into the Future, 2010, Available from: http://www.motorbooks.com/.
[7] N.A. Kelly, T.L. Gibson, D.B. Ouwerkerk, International Journal of Hydrogen Energy 33 (2008) 2747–2764.
[8] T.L. Gibson, N.A. Kelly, International Journal of Hydrogen Energy 33 (2008) 5931–5940.
[9] T.L. Gibson, N.A. Kelly, International Journal of Hydrogen Energy 35 (2010) 900–911.
[10] N.A. Kelly, T.L. Gibson, D.B. Ouwerkerk, International Journal of Hydrogen Energy 36 (2011) (1580) 3–15825.
[11] N.A. Kelly, T.L. Gibson, M. Cai, J.A. Spearot, D.B. Ouwerkerk, International Journal of Hydrogen Energy 35 (2010) 892–899.
[12] T.L. Gibson, N.A. Kelly, Journal of Power Sources 195 (2010) 3928–3932.
[13] N.A. Kelly, T.L. Gibson, Journal of Power Sources 196 (2011) 10430–10441.
[14] G.W. Crabtree, N.S. Lewis, Physics Today 60 (2007) 37–42.
[15] J.A. Turner, Science 305 (2004) 972–974.
[16] J.A. Turner, G. Sverdrup, M.K. Mann, P.C. Maness, B. Kropski, M. Ghirardi, R.J. Evans, D. Blake, International Journal of Energy Research 32 (2008) 379–407.
[17] W.J. Kempton, J. Tomic, Journal of Power sources 144 (2005) 280–294.
[18] G. Gutmann, Journal of Power Sources 84 (1999) 275–279.
[19] DOE, Report from Workshop sponsored by U.S. Department of Energy, Office of Electricity Delivery and Energy Reliability, Available from: http://www.oe.energy.gov/DocumentsandMedia/Utility_12-30-10_FINAL_lowres.pdf.

[20] Sanyo Energy (USA) Corp., HIT Series Data Sheet, HIP-190BA3, http://www.us.sanyo.com/solar/.
[21] N.A. Kelly, T.L. Gibson, Solar Energy 85 (2011) 111–125.
[22] PEVE Battery, Available from: http://www.peve.jp/e/hevjyusi.html.
[23] M. Thele, O. Bohlen, D. Uwe Sauer, E. Karden, Journal of Power Sources 175 (2008) 635–643.
[24] M. Verbrugge, J. Tate, Journal of Power Sources 126 (2004) 236–249.
[25] X. Tang, X. Zhang, B. Koch, D. Frish, Proceedings of International Conference on Prognostics and Health Management, Denver, CO, 2008.
[26] F. Xuyun, S. Zechang, IEEE Vehicle Power and Propulsion Conference (VPPC), Harbin, China, September 3–5, 2008.
[27] X.G. Yang, B.Y. Liaw, Journal of Power Sources 102 (2001) 186–197.